lubricants

MDPI

Article

Misalignment-Induced Micro-Elastohydrodynamic Lubrication in Rotary Lip Seals

F. Xavier Borras *, Matthijn B. de Rooij and Dik J. Schipper

University of Twente, Surface Technology and Tribology, 7522NB Enschede, The Netherlands; m.b.derooij@utwente.nl (M.B.d.R.); d.j.schipper@utwente.nl (D.J.S.)

* Correspondence: f.borrassubirana@utwente.nl; Tel.: +31-053-489-5300

Received: 15 January 2020; Accepted: 29 January 2020; Published: 10 February 2020

Abstract: In literature the lubrication of rotary lip seals is explained by hydrodynamic action on a microscopic scale. This theory assumes perfect concentricity between the seal and the shaft which in reality seldomly occurs. Focusing on the stern tube seals application, an analysis is performed on the phenomena distorting the axisymmetric operation of rotary lip seals. Radial and angular shaft misalignments together with pressure and temperature gradients have been modelled. The model predictions are validated using a dedicated setup. Additionally, applying the soft-EHL film thickness expressions at the asperity level, an equivalent film thickness along the circumferential direction is estimated. The Reynolds PDE is solved to predict the misalignment-induced hydrodynamic pressure build-up. The film thickness variation derived and accompanying non-uniform contact pressure distribution was shown to be sufficient for hydrodynamic action and, depending on the minimum film thickness, the hydrodynamic pressure build-up can exceed the static contact pressure. Additionally, significant differences were observed between the radial and angular misalignment configurations.

Keywords: EHL; film thickness; rotary; lip seal; misalignment; stern tube; seal

1. Introduction

The working mechanism of lubricated rotary lip seals have been the subject of discussion for the past decades. The presence of some sort of hydrodynamic action is repeatedly reported in literature. Jagger [1] was the first one to notice that the frictional torque of rotary lip seals included a viscous component, i.e., the friction between the shaft and the seal was inherently coupled to the turning velocity. His findings could explain the extremely low wear rates observed in some rotary lip seals [2]. Later Stakenborg [3] observed air bubbles arising from the sealing contact when running. The location of the cavitation area varied with the shaft angular speed. Wennehorst [4], among others, measured the lift-off of the seal lip with increasing shaft speed. While it is a given that a hydrodynamic film (partial or full) is present, the following two questions posed by Salant [5] prevail: what is the origin of the fluid hydrodynamic pressure built-up? If surface separation partially or fully develops, why does the seal not leak?

Contrasting with journal bearings and thrust bearings, lip seals do not present a convergent gap profile, i.e., a wedge, in the direction of motion in the absence of misalignment. Therefore, no pressure build-up is expected from the operation of a perfectly concentric seal [4]. Lip seals resemble mechanical shaft seals in the sense that both require deviations from nominal parallelism to generate an hydrodynamic load support. Ever since the presence of hydrodynamics was first documented, researchers have theorized about the mechanism behind rotary lip seals. Several theories, both macroscopic and microscopic [6], able to explain the almost leak-less and wear-less operation of lubricated rotary lip seals have been presented in literature.

Up to now, the generally accepted theory relies on the hydrodynamic action on the microscopic level to explain the performance of rotary lip seals. When the shaft rotates, the microscopic wedges between the seal and shaft surface asperities generate a hydrodynamic fluid load carrying capacity capable of partially or fully supporting the radial force of the seal lip. Furthermore, the compressed asperities are tangentially distorted in the circumferential direction due to friction leading to a shaft-seal topography resembling a micro-screw pump [5] (see Figure 1). Consequently, in a similar fashion as a visco-seal, the rotation of the shaft induces a flow in one direction preventing the leakage in the opposite direction. This sealing mechanism is known as the reverse, upstream or back pumping of rotary lip seals [6]. When running on an oil–air interface, the ingress of air is often described in literature [7].

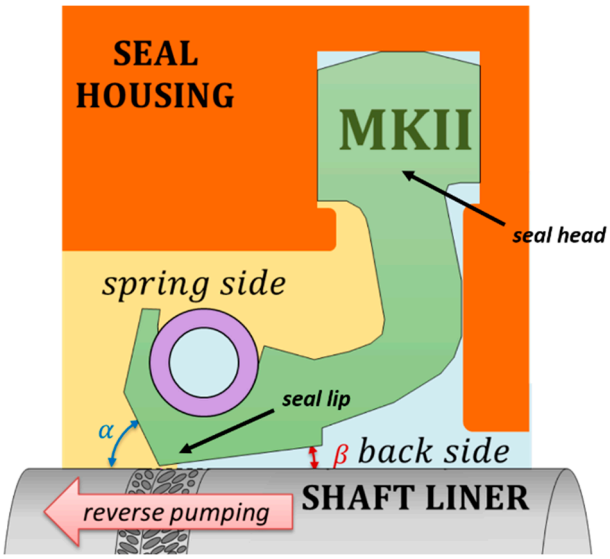

Figure 1. Characteristic reverse pumping mechanism or rotary lip seals.

Although the microscopic theory can explain many of the phenomena observed in rotary lip seals [5], it disregards the shaft-seal misalignment which has repeatedly shown to play a significant role when it comes to wear rate, contact temperature, and the lifespan of sealing components [8]. The loss of the seal–shaft concentricity is usually classified between radial and angular misalignments [9]. Radial misalignment refers to the offset between the bore and shaft axes (parallel misalignment), i.e., keeping the axes parallel. The second type of misalignment, also known as skewness, cocking, cant or slant, refers to the difference in orientation between the shaft and bore axes. Both radial (ε) and angular (θ) misalignments can be constant (static) or variable in time (dynamic). The four possible configurations are shown in Figure 2. The loss of nominal parallelism between the seal and the shaft can result from the bearings internal and mounting clearances, the shaft out-of-roundness, the manufacturing tolerances, the radial vibrations, the shaft loading or the speed-induced wobbling of the shaft [10]. The viscoelasticity of the seal material affects the followability of the seal [11] and it will also lead to a misaligned operation [12]. Poll [13] presented torque measurements of a seal oscillating at the rotation frequency of the shaft. This is a clear consequence of dynamic misalignment between the seal and the shaft.

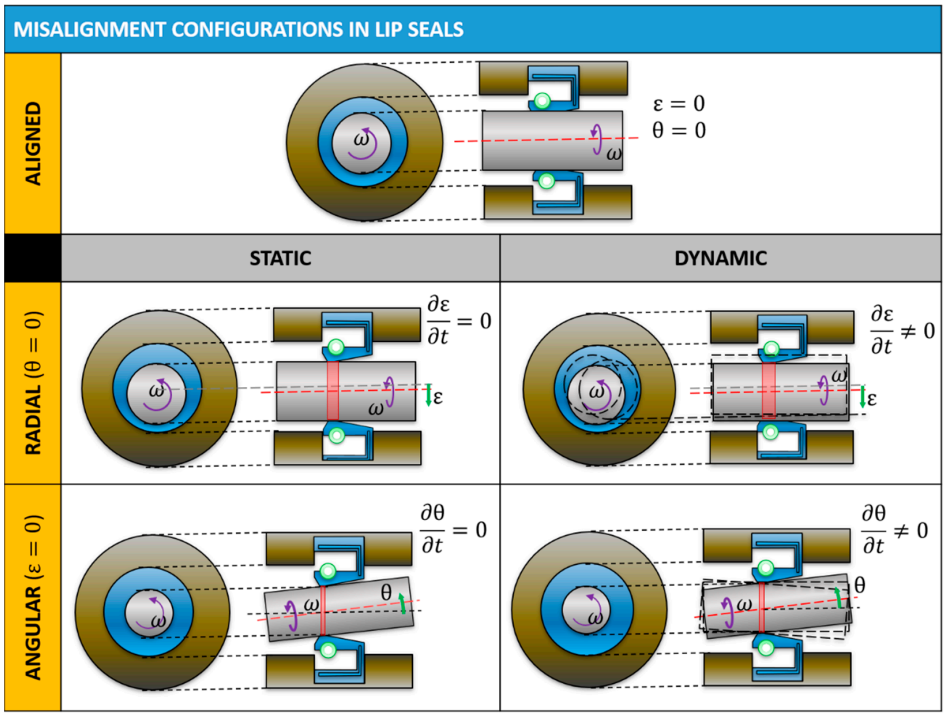

Figure 2. Classification bore-to-shaft misalignment in lip seals.

While there are methods to measure the sealing force of a radial seal [14], there is not a standard way to measure it when the seal and the shaft are offset. The overall reaction force to a set of radial misalignments were measured by Tasora [15] and Pinedo [16]. Their measurements show good agreement with the loads obtained using the Finite Elements (FE) models. Van Babel [17] sketched the resultant contact area from both radial and angular misalignments showing that, the tip of the seal is axially displaced as a result of it. This phenomenon is shown in Figure 3.

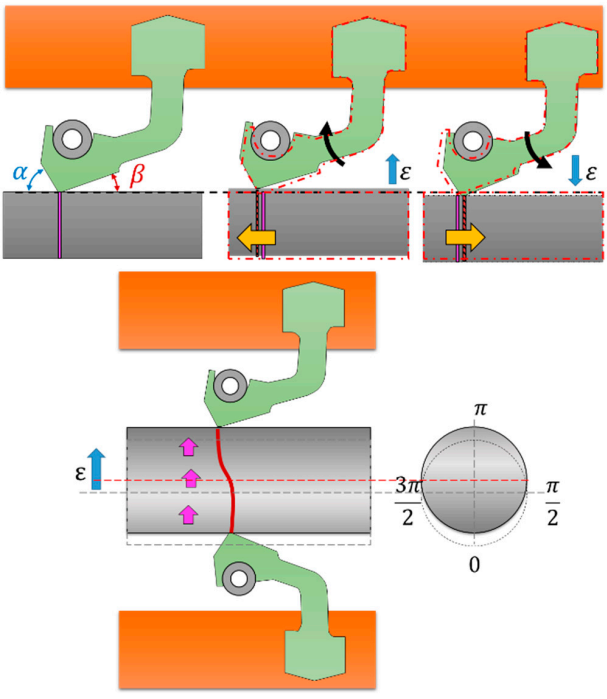

Figure 3. Tip axial displacement induced by the shaft offset.

Here a particular type of a stern tube seal of 200 mm nominal diameter is analysed. For this application, the large dimensions of the components of the propulsion system, the manufacturing accuracy of the elastomeric parts together with the inherent offset with the shaft bearings [18] make the bore-seal misalignment more than probable. Nevertheless, less obvious effects might also lead to a non-concentric shaft operation. Stern tube seals operate below the seawater level thereby subjected to hydrostatic pressure. Furthermore, as the seals are vertically positioned, there is a hydrostatic pressure gradient from the highest to the lowest point of each seal. The pressure difference is directly related to the diameter of the seal. As a result of it, stern tube seals can present a skewed contact profile. Ultimately, Arai [10] showed the sensitivity of the seal to temperature variations due to the large thermal expansion of elastomers. He reported about seals which were only tight beyond a particular temperature. Sinzara [19], using an IR camera, showed a significant temperature gradient along the perimeter of the seal contact when the shaft was intentionally offset.

The actual film thickness of rotary lip seals, which would clarify their actual lubrication regime, still remains difficult to measure. The film thickness values shown in literature span from 0.1 to 10 μm and significant changes to the tribo-system are required to make the measurements feasible. Organisciak [20] fitted a function to the lubricant film thickness measurements of radial shaft seals for gearboxes showing a fair resemblance to the iso-viscous elastic film thickness expressions (soft-elastohydrodynamic lubrication [21]). Fowell [22] measured the film thickness of fluoroelastomer specimens using the laser induced fluorescence (LIF) technique and these showed to be in good agreement with Hamrock [21] and Nijenbanning [23] elastohydrodynamic lubrication (EHL) models. First Gabelli [24] and then Wennehorst [4] made use of the Chittenden expressions [25] to predict the minimum film thickness on rotary lip seals by applying it at the microscopic level, i.e., for a single asperity contact. Wennehorst recently managed to measure the film thickness on a rotary lip seal using the LIF technique [4].

The contact pressure and area resulting from different misaligned configurations are obtained. Next, the effects of the temperature difference over the seal as well as the presence of a hydrostatic pressure gradient will be analyzed. Further, the authors applied the soft-EHL theory to estimate the equivalent gap profile between the shaft and the seal. Ultimately, the seal is modelled as a journal bearing to estimate the hydrodynamic pressure expected from a misalignment-induced gap profile.

2. Materials and Methods

The strategy for modelling the hydrodynamics developing under a non-concentric shaft-seal configuration counted with the three steps shown in Figure 4. The first step consisted in estimating the contact pressure and contact area on a misaligned configuration. Subsequently, specifying a shaft angular velocity and a lubricant viscosity, the soft-EHL theory was applied resulting in a lubricant film thickness along the circumferential direction. Ultimately, by solving the Elrod–Addams algorithm in the film thickness profile obtained (i.e., under the same operating conditions), the hydrodynamic pressure build-up was predicted.

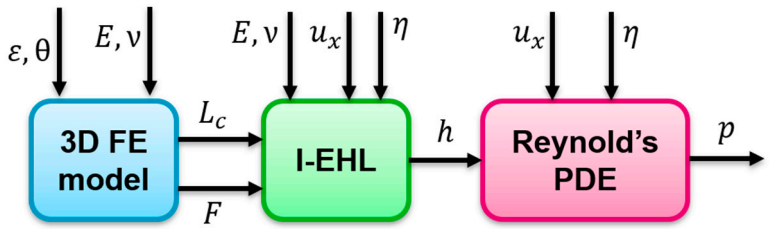

Figure 4. Scheme of the modelling strategy (see Nomenclature).

A stern tube seal FE model was developed to study the response of a lip seal to various kinds of misalignments. The commercial FE package COMSOL Multiphysics® was used to model a 200 mm stern tube seal. The contact force, contact area and pressure profile under the seal tip were predicted using the large strain theory and modelling the seal with the Saint Venant–Kirchoff constitutional

material model with the properties listed in Table 1. The lack of axial symmetry of the loads required the use of a three-dimensional model [15,16]. Therefore, the axisymmetric approach presented in a previous publication of the authors [14] was extended along the circumferential direction. The initial configuration was considered to be the one with the seal head already clamped between the seal housing components (see Figure 1). It is essential to model the clamping stage as the inner diameter of the seal lip decreases as a result of it. The seal head boundary nodes were consequently fixed leading to a model with a single boundary contact (instead of four [14]).

Table 1. Material properties used in the three-dimensional stern tube seal FE model.

		Stern Tube Seal	**Shaft**	**Seal Housing**
E	[MPa]	14.0	2.0×10^5	1.065×10^5
ν	[−]	0.49	0.27	0.35
ρ	$\left[\mathrm{kg/m^3}\right]$	1900	7700	8800
C_p	[J/(kg·K)]	1670	1909.7	376
k	[W/(m·K)]	0.25	25	60
α_T	[1/K]	2.75×10^{-4}	1.0×10^{-5}	1.85×10^{-5}

The frictionless penalty term method was used easing the overall convergence of the model. This method allows for a certain body penetration leading to slightly lower maximum contact pressures than when using the augmented Lagrangian method. Due to that, the stiffness listed in Table 1 was obtained by matching the model predictions to the actual radial force measurements conducted using the split-shaft setup shown in Figure 5 [14]. The tangential load at the contact was shown to not significantly impact the contact pressure nor the contact width for a seal with the material properties as given in Table 1.

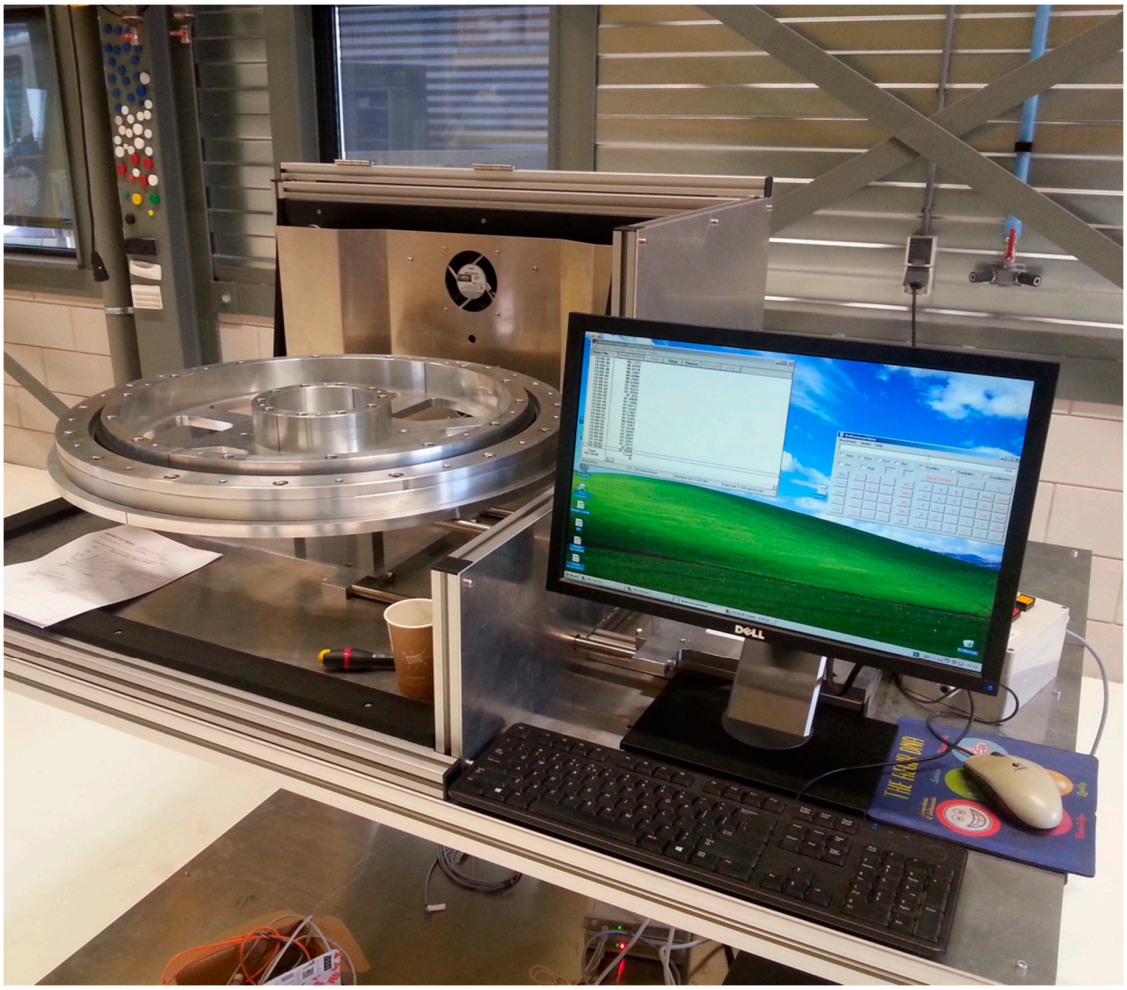

Figure 5. Split-shaft setup used for measuring the radial force exerted by the stern tube seal.

The radial and angular static misalignments were implemented by prescribing the displacement of a rigid shaft as depicted in Figure 2. The hydrostatic pressure was modelled as a true follower load coupled to the x direction in Figure 6. The symmetric nature of the components and the misalignments allowed to only model half the seal. For the study of hot spots, the temperature at the tip of the seal was prescribed as a boundary condition and the energy equation was solved using the same convective coefficients as used by Stakenborg [3] while the surrounding temperature was set to 20 °C. A quad element mesh was used for the seal and shaft sections. A high degree of mesh refinement on the circumferential direction was required so the pressure profile of the three-dimensional model matched with the one obtained when using an equivalent axisymmetric model.

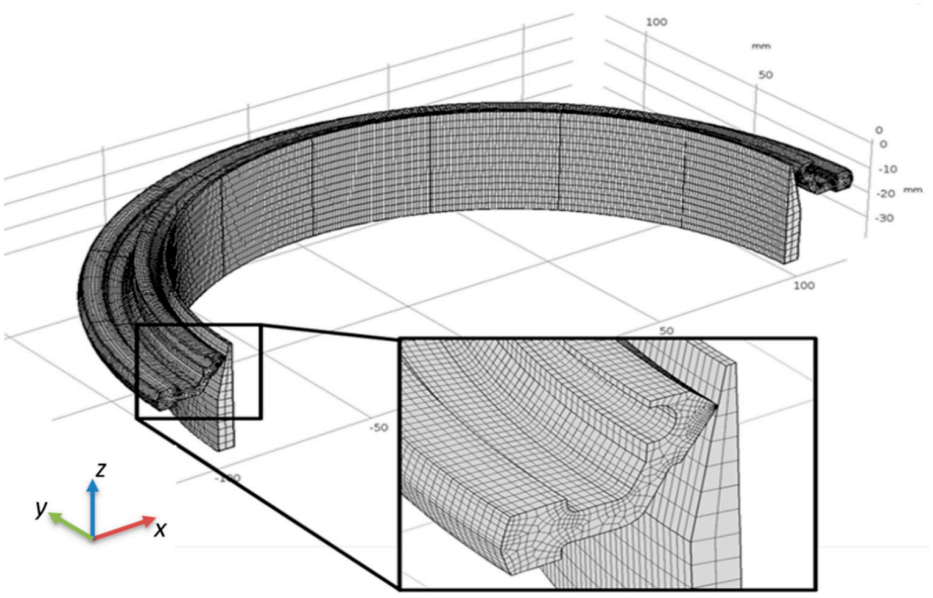

Figure 6. Three-dimensional model of the seal. Note the taper shaft part required for its concentric assembly.

The dedicated setup schematically shown in Figure 7 was developed allowing to measure the contact area between the seal and the shaft. The setup is equipped with a glass shaft which allows for the direct inspection of the contact area. A precision camera (Dino-Lite, Taiwan, China) and a 45 degrees mirror are assembled on a turning table allowing to directly observe the contact area along the complete perimeter of the seal. The Frustrated Total Internal Reflection technique is used to ease the visualization of the contact [4,14]. The setup also allows the housing parts (and the seal) to slide with respect to the glass shaft so a static offset can be simulated. The test rig was used to validate the predictions of the FE model.

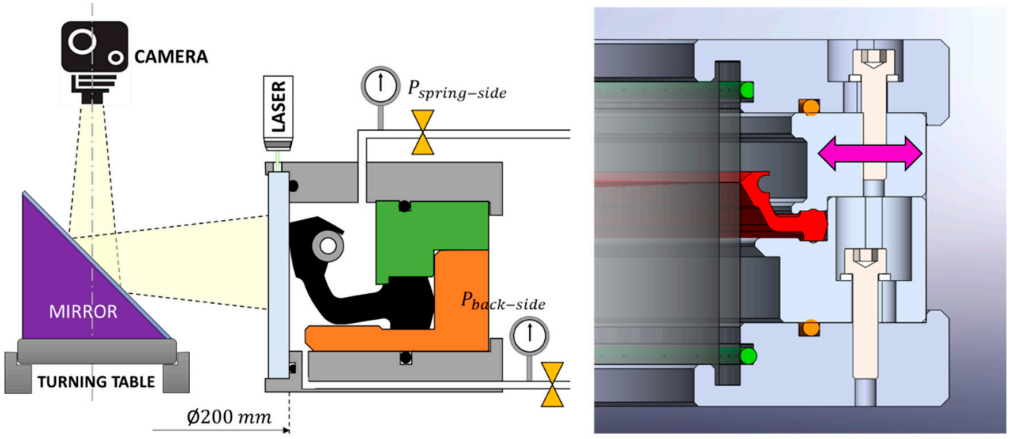

Figure 7. Specialized seal setup to observe the seal contact under various misalignments and pressurized conditions.

Once the reliability of the model was ascertained and in agreement with Gabelli [24] and Wennehorst [4], the iso-viscous elastohydrodynamic film thickness expression (soft-EHL or I-EHL) introduced by Chittenden [25] was used to estimate the film thickness profile between the seal and the shaft under real operating conditions (Equations (1)–(4)). The angle between the lubricant entraining vector and the major axis of the asperities was considered to be low enough to disregard its impact to the fluid film thickness.

$$\frac{h_{cen}}{R_x} = 8.28\left(1 - e^{-0,86\left(\frac{R_y}{R_x}\right)^{2/3}}\right) U_x^{0,65} W_x^{-0,21} \tag{1}$$

$$U_x = \eta u_x / (E' R_x) \tag{2}$$

$$W_x = F / (E' R_x^2) \tag{3}$$

$$E' = \frac{2}{\frac{(1-v_1^2)}{E_1} + \frac{(1-v_2^2)}{E_2}} \tag{4}$$

Equation (1) predicts the central film thickness h_{cen} in elliptical conjunctions. Due to the lack of a radius of curvature in the entrainment direction of rotary lip seals, no pressure can be generated in circumferential directions. However, at the microscopic level, the radius of curvature can be defined. In order to model micro-hydrodynamic pressure generation, the I-EHL formula is applied at the asperity level. The seal surface roughness was scanned with lateral sampling intervals in both directions of 0.217 µm using a confocal microscope (Sensofar, Barcelona, Spain). From the surfaces roughness measurements, the effective wavelength $\lambda_{x/y}$ and the equivalent radius $R_{x/y}$ were obtained by applying Equations (5) and (6) in agreement with Wennehorst [4].

$$\lambda_{x/y} = 2\pi \frac{S_q}{\Delta_{x/y}} \tag{5}$$

$$R_{x/y} = \frac{1}{\sqrt{2}\, S_q} \left(\frac{\lambda_{x/y}}{2\pi}\right)^2 \tag{6}$$

Neither the contact pressure nor the contact area are uniformly distributed in the circumferential direction when the system is misaligned. Therefore, the number of asperities in the axial direction becomes the ratio between the contact width L_c and the effective wavelength λ_y. The loading of each asperity is obtained by uniformly distributing the contact pressure over the number of asperities in the axial direction (see Figure 8). The equivalent film thickness is defined as the I-EHL central film thickness h_{cen}. It is worth emphasizing that full film lubrication is assumed hence direct asperity contact does not occur and the so-called asperity load is fully carried by the micro-hydrodynamic pressure.

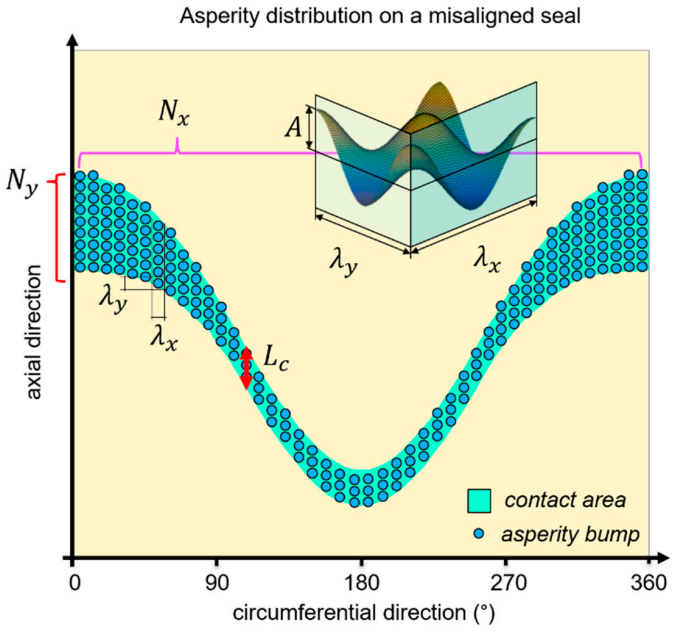

Figure 8. Distribution of asperities on the contact area profile of a slanted seal (see Nomenclature).

Ultimately, the two-dimensional mass-conservative Elrod–Adams Reynolds formulation (Equations (7)–(9)) was solved on the gap profile obtained from the I-EHL film thickness expression. In the simulations, the contact width, the lubricant viscosity and density were kept constant in the computational domain. Further information on the strategy for solving the partial derivative equation can be found in [26]. The hydrodynamic pressure built-up induced by a non-uniform pressure distribution along the circumferential direction was then predicted. A sensitivity analysis of the minimum film thickness and the contact width is shown in the results section.

$$p = p_c + g\beta \ln(\phi) \tag{7}$$

$$\frac{\partial}{\partial x}\left(\frac{g\beta h^3}{12\eta}\frac{\partial \phi}{\partial x}\right) + \frac{\partial}{\partial y}\left(\frac{g\beta h^3}{12\eta}\frac{\partial \phi}{\partial y}\right) = \frac{u_x}{2}\frac{\partial(\phi h)}{\partial x} \tag{8}$$

$$full\ film\ zone\begin{cases} \phi > 1 \\ g = 1 \end{cases} \qquad cavitation\ zone\begin{cases} \phi < 1 \\ g = 0 \end{cases} \tag{9}$$

The strategy described allows to predict the impact of operating with a non-uniform contact pressure distribution in the circumferential direction for rotating conformal contacts. Note that the additional deformation of the seal tip due to the hydrodynamic action is disregarded in the approach discussed above and hence lower pressure values are expected in the real application.

3. Results

The deformed seal configurations as a result from the radial and angular misalignments are presented in Figure 9. On the top plots, the black arrows indicate the displacement of the shaft. In the figure, the seal is colored according to the magnitude of the seal displacement. On the bottom plots the displacement of the seal in axial direction with respect to the assembled concentric situation is shown. Figure 10 shows the magnitude of the displacements under various misalignments.

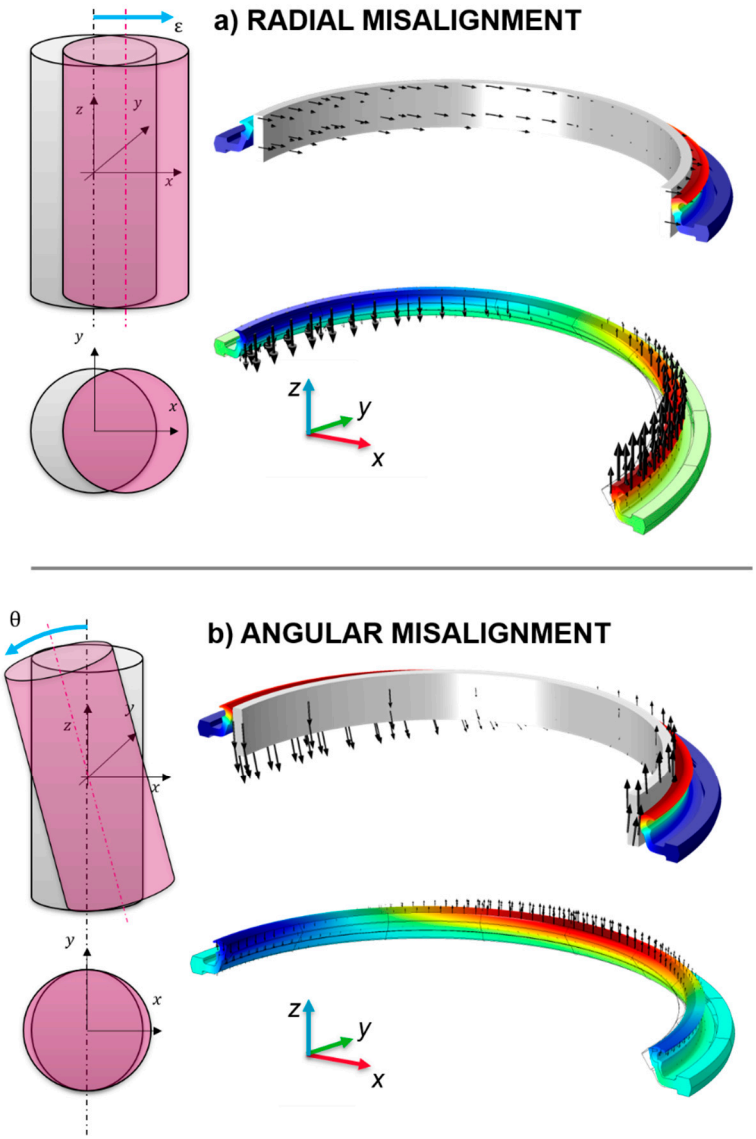

Figure 9. Seal displacement due to radial (**a**) and angular (**b**) misalignments.

The contact area profiles obtained under radial misalignment coincide with the schematic sketch presented by Van Bavel [17] however the contact area under angular misalignment does not. As it was observed with O-rings [27], under angular misalignment, the sealing section becomes oval increasing the diameter of the shaft on the direction of misalignment (see Figure 9). A negative axial displacement of the lip occurred where the diameter was enlarged and a displacement in the opposite direction developed where the diameter remained constant. As shown in Figure 10 the lip displacement under angular misalignment was smaller than under radial misalignment. Note that while a radial misalignment produced one sinus-shaped profile, an angular misalignment led to two sinus shaped profiles along the circumference. Using the setup shown in Figure 7 the contact area profile under radial misalignment was validated. The amplitude of the contact profile shows good agreement with the FE model predictions (see Figure 10). The calculated radial contact force along the circumferential direction is shown in Figure 11. It is shown that the pressure variation along the circumferential direction for the largest radial misalignment case ($\varepsilon = 1.5$ mm) oscillated by 20% with respect to its aligned position. For the largest angular misalignment modelled ($\theta = 2°$) the pressure variation only varied 1%.

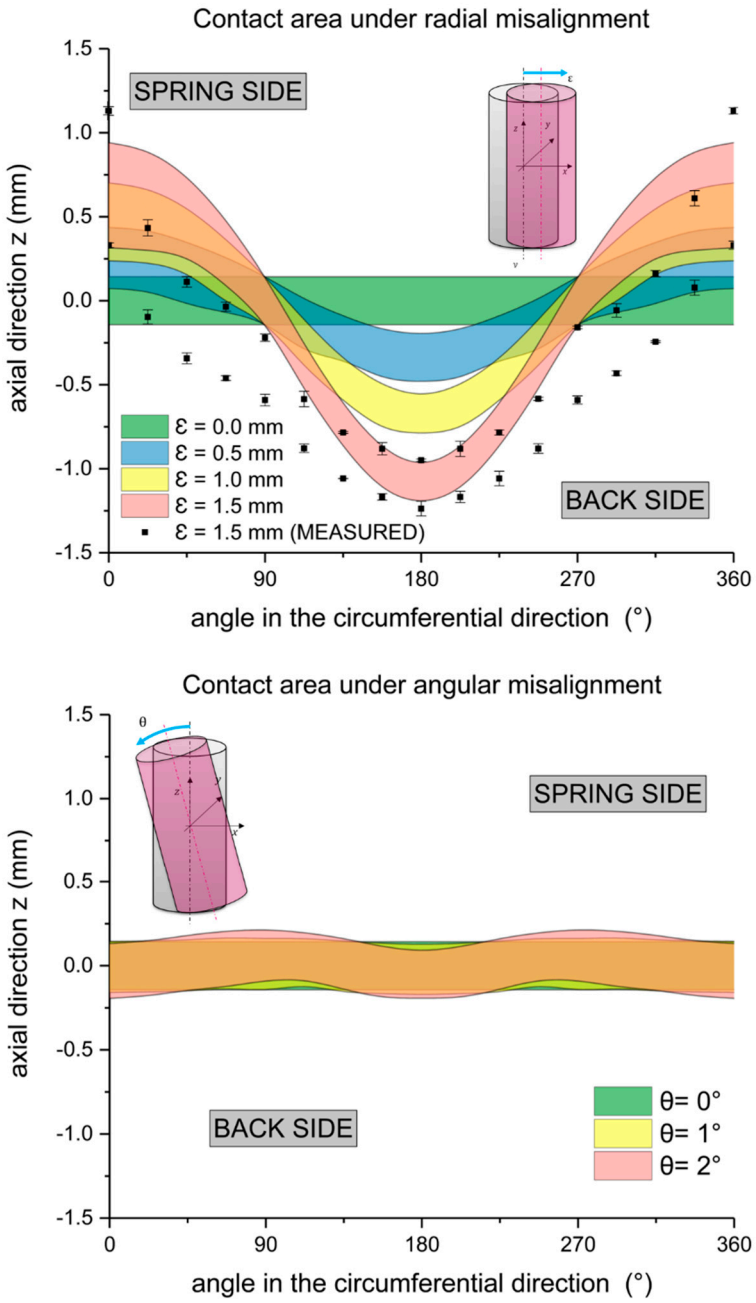

Figure 10. Contact area around the shaft for various radial and angular misalignments.

When the hydrostatic pressure gradient was modelled as a boundary condition the displacements obtained were minimal even under frictionless conditions. Therefore, the seal–shaft misalignment due to the hydrostatic pressure gradient was found neglectable for this particular seal with a nominal diameter of 200 mm.

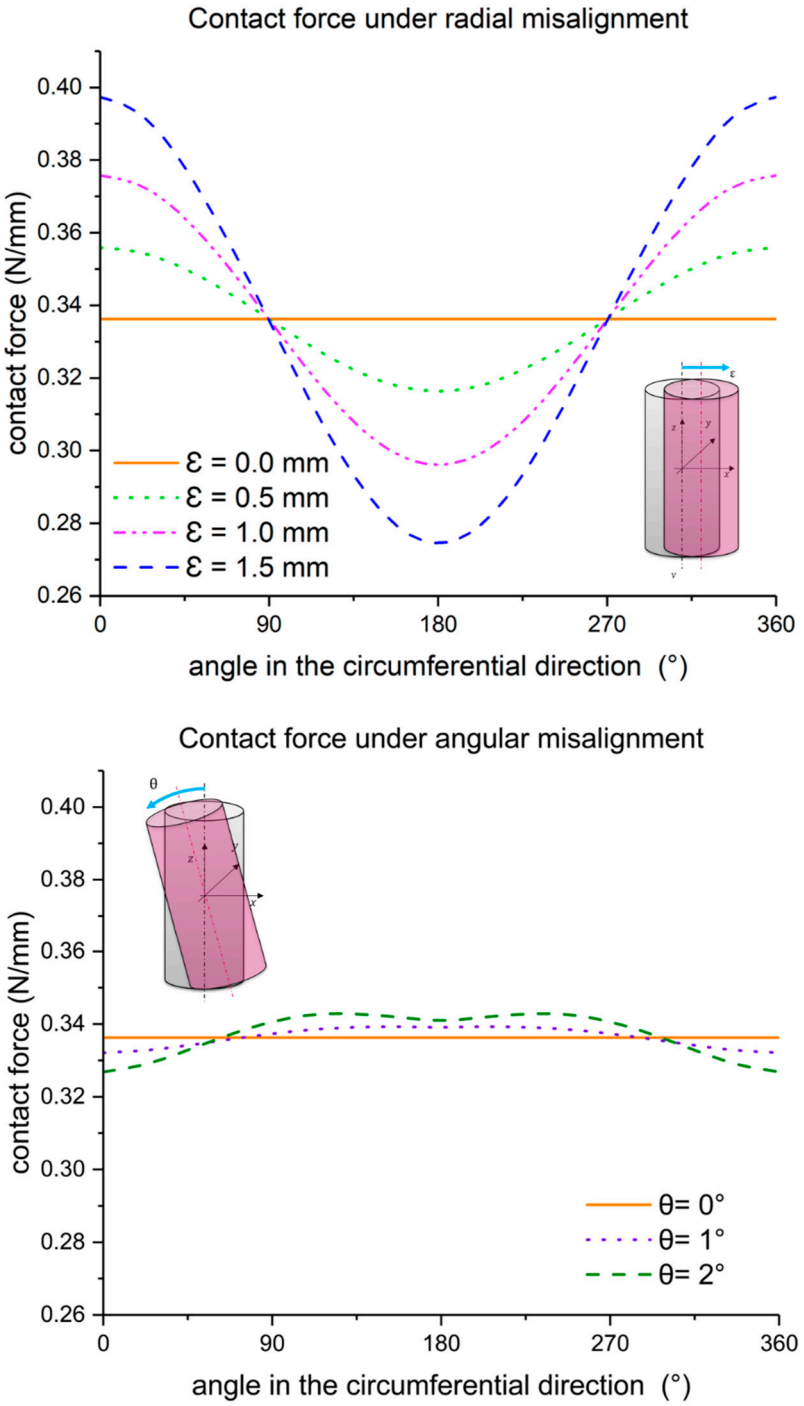

Figure 11. Contact force around the shaft for various radial and angular misalignments.

Lastly, the effect of temperature differences along the circumference is analyzed. Such temperature difference can possible occur due to local frictional hot spots, leading to localized frictional heating. If temperature differences are present, the consequences will be magnified due to the large thermal expansion coefficients of elastomers. The presence of warmer points on the seal contact, i.e., hot spots, results into a non-uniform thermal expansion of the seal tip leading to a distorted gap profile [19]. The thermal distortion of the seal lip when a temperature gradient developed at the contact of a perfectly aligned seal was modelled. Hence the sole impact of temperature was captured and it is shown in Figure 12. The temperature gradient was defined along the contact area of the seal as a

temperature boundary condition while a heat convection to a 20 °C surrounding was set for the rest of the seal boundaries. Figure 12 shows that with a temperature gradient of 20 °C along the seal contact the thermal expansion only slightly distorted the seal alignment, both the contact area and the contact pressure became larger at the warmest section of the seal.

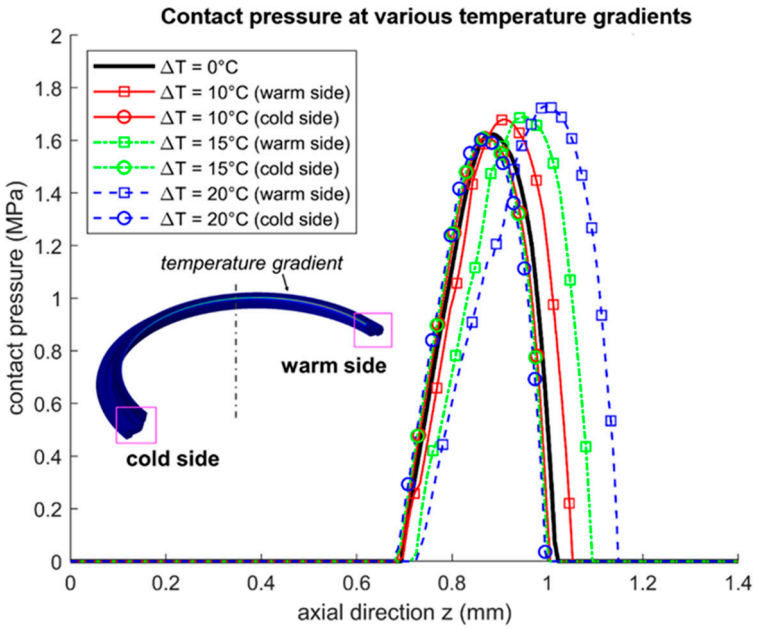

Figure 12. Impact of a contact temperature gradient along the seal perimeter.

Next, the film thickness along the circumferential direction was predicted for the 1.5 mm radial misalignment case. The worn surface topography scanned presented the following surface roughness parameters: $S_q = 1.24$ µm, $\Delta_x = 0.217$ µm and, $\Delta_y = 0.275$ µm (see Nomenclature). Figure 13 shows the average load that the micro-hydrodynamic pressure generated at each asperity together with the film thickness obtained by applying the I-EHL formulae (Equations (1)–(4)). It is shown that the maximum hydrodynamic load was approximately three times the minimum one while the difference between the maximum and minimum film thickness was just of the order of 100 nanometers.

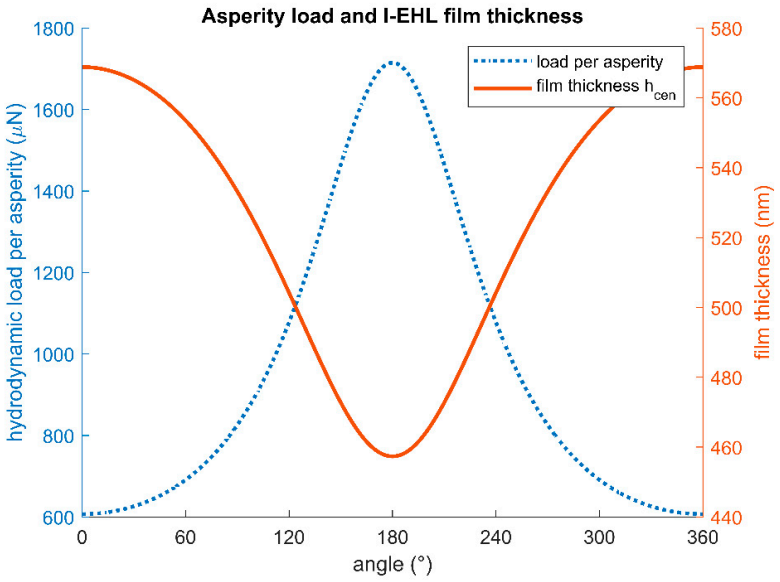

Figure 13. Asperity loading and fluid film thickness for the seal with a 1.5 mm radial misalignment offset.

Ultimately, the 2D Elrod–Addams equation (Equation (7)) was solved on the I-EHL film thickness profile shown in Figure 13 so the hydrodynamic pressure build-up for the 1.5 mm radial misalignment situation was predicted. Figure 14 shows that the resultant hydrodynamic pressure profile was one order of magnitude smaller than contact pressure and hence it cannot be directly disregarded.

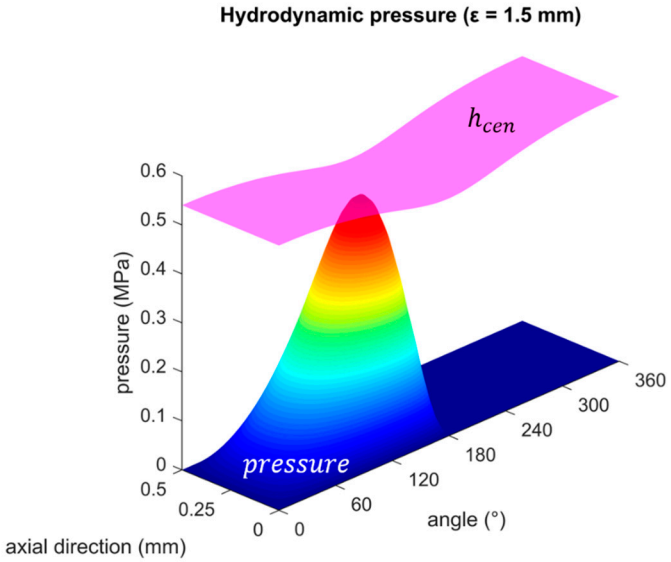

Figure 14. Hydrodynamic pressure build-up under radial misalignment offset ($\varepsilon = 1.5$ mm, $\eta = 100$ mPa·s, $\beta = 1.0 \times 10^7$ Pa, $u_x = 1$ m/s, $L_c = 0.5$ mm). The I-EHL film thickness from Figure 13 is magnified and shown in pink.

To study the dependency of the lubricant film profile to the hydrodynamic pressure generation both the minimum film thickness (Figure 15) and the contact width (Figure 16) are varied while keeping the film thickness gradient deduced from I-EHL (see Figure 13). Both the minimum film thickness and the contact width were shown to be key parameters to the seal operation. It is observed that, for some cases, the hydrodynamic pressure build-up (disregarding the lip deformation) overcame the static contact pressure and hence it largely impacted the lubrication mechanism of rotatory lip seals.

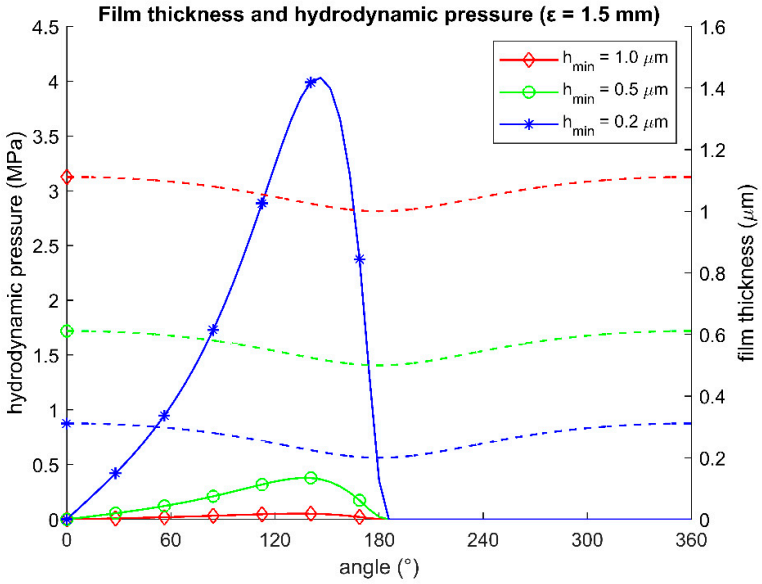

Figure 15. Minimum film thickness sweep ($\varepsilon = 1.5$ mm, $\eta = 100$ mPa·s, $\beta = 1.0 \times 10^7$ Pa, $u_x = 5$ m/s, $L_c = 0.5$ mm).

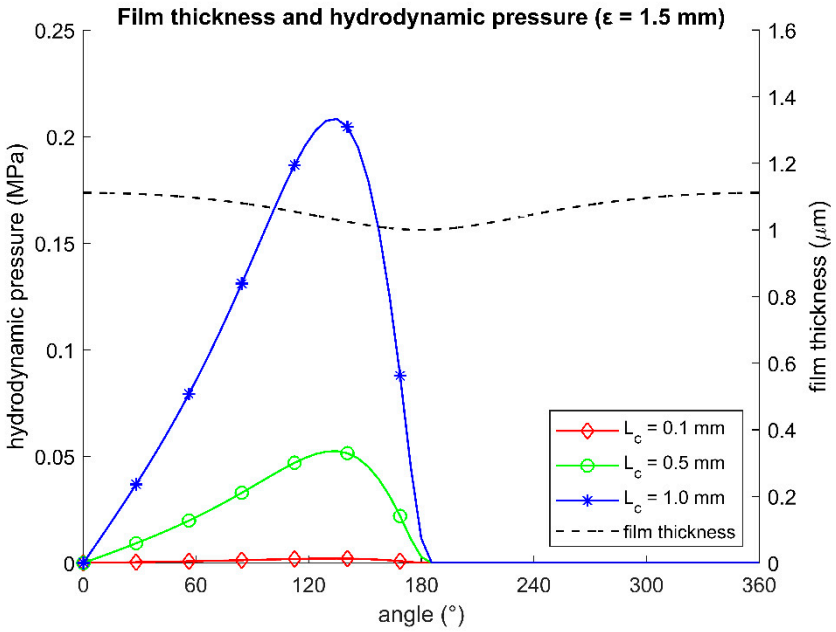

Figure 16. Contact width L_c sweep with the I-EHL film thickness variation ($\varepsilon = 1.5$ mm, $\eta = 100$ mPa·s, $\beta = 1.0 \times 10^7$ Pa, $u_x = 5$ m/s, $h_{min} = 1$ μm).

4. Discussion

Various mechanisms leading to a non-concentric operation of stern tube seals were analyzed. The radial misalignment was shown to distort the axial symmetry of the system more significantly than the angular one (skewness). Under real operating conditions a combination of both misalignments is to be expected. On the same line, the contact area and pressure did minimally vary for the canted seal. An angular misalignment of 2° is several times larger than the maximum slope mismatch expected in the aft stern tube bearing under free-sailing condition [28]. However, the length and diameter of the shaft is ship-dependent and the distance from the stern tube bearing to the sealing rings may lead to a larger angular misalignment. Additionally, assembling or manufacturing defects may also result in a shaft-seal non-concentric operation. The contact area measurements showed to be in good agreement with the FE model predictions. The use of a linear elastic model for the seal and the simplification of the seal boundary conditions can explain the slight differences observed between the model and the experiments. The sinusoidal and double-sinusoidal contact profiles along the circumference will lead to an axial flowrate promoting the lubrication of the seal. The swept contact area is in both cases increased so lower contact temperatures are expected. Although time-dependent effects were out of the scope of this research, the viscoelasticity of the material will play a significant role under dynamic misalignment, e.g., wobbling [11,12,29]. The difference in pressure between the top and bottom part of the 200 mm seal, i.e., around 0.02 bar pressure difference, did not significantly distort the alignment of the system. Note that the hydrostatic pressure difference increases with the shaft diameter and its contribution to the seal slant must be then re-evaluated when working with larger seals. The large thermal expansion coefficient of the seal material was shown to impact the position of the seal tip. Although the temperature of the seal is expected to even out on the long term, during its transient state, the temperature gradient promotes a wedge profile and therefore hydrodynamics.

The use of EHL film thickness expressions [21] for a conformal contact has its uncertainties and limitations [4]. Nevertheless, these formulae is used to evaluate the hydrodynamic potential arising from a misaligned shaft-seal situation. Furthermore, the magnitude of the film thickness predicted is in fair agreement with the ones found in literature. For the largest case of radial misalignment, i.e., 1.5 mm offset, the maximum hydrodynamic load per asperity is 2.82 times larger than the minimum one. The maximum film thickness calculated with Equation (1) becomes only 1.24 times larger than

the minimum one. That is because the loading of the junction does not significant impact the film thickness according to the I-EHL formulations revised [21,23,25]. Note that, in some particular cases, the contact area can increase further than the contact pressure on the loaded side of the seal. This leads to the counterintuitive situation where the asperities on the uncompressed side of the seal bear the largest loads.

The hydrodynamic pressures predicted from modelling a rotary lip seal as a slender journal bearing (Equation (7)) showed to be of the same order of magnitude than the static contact pressures [14]. Note that such peak pressure values will not develop as the seal deforms as a result of it. Some authors [5] suggested that a varying contact pressure, whether due to the coils separation of the Garter spring or due to the molding of hydrodynamic ribs, generates a secondary load pressure build-up mechanism. The same may occur due to the inherent viscoelasticity of the seal material [11,12]. The analysis shows that minute gap gradients suffice to generate a significant hydrodynamic action and that, together with the minimum film thickness and the contact width, impacts the normal operation of rotary lip seals. Furthermore, if such macroscopic hydrodynamic pressures develop, the micro-elastohydrodynamic working principle behind rotary lip seals will be distorted. As it occurs with visco-seals, the pumping ability vanishes with the alignment of the shaft. When it comes to modelling, the widely used approach presented by Salant [4,5] analyzes a single patch (i.e., cell) of the seal surface and the results are extrapolated to the rest of the contact, i.e., these cells are assumed to be periodic along the circumferential direction. However, when the pressure is not uniformly distributed along the circumferential direction, each surface patch operates under unique operating conditions and hence each patch must be independently evaluated.

It is worth mentioning that the sinus-shaped contact area will further promote the hydrodynamic action. The slant of the contact area unequivocally leads to a normal-to-the-contact shaft velocity component (hereby omitted). Although an early model accounting for this velocity component is available [8], a more advanced hydrodynamic model is required to accurately consider it.

5. Conclusions

Four different mechanisms distorting the axisymmetry of rotary lip seals were studied: radial and angular misalignments, the hydrostatic pressure gradient and the presence of hot spots at the seal contact. Both shaft misalignments and thermal expansion were found to contribute to hydrodynamic pressure build-up. On the other hand, the hydrostatic pressure differences between the top and the bottom of a stern tube seal do not significantly influence hydrodynamic effects for the stern tube seal studied. The radial and angular misalignments showed substantial different contact profiles. The misalignment-induced hydrodynamics arising from the equivalent film thickness profile were shown to be significant. This pressure build-up was shown to be extremely sensitive to the minimum film thickness and contact width. The results show that the assumption of periodic cells on the circumferential direction when modelling rotary lip seals must be reviewed for misaligned configurations.

Author Contributions: Conceptualization, F.X.B.; Investigation, F.X.B.; Supervision, M.B.d.R. and D.J.S.; Writing—original draft, F.X.B.; Writing—review & editing, M.B.d.R. and D.J.S. All authors have read and agreed to the published version of the manuscript.

Funding: This research received no external funding.

Acknowledgments: Rob Dierink, Eric de Vries, Robert-Jan Meijer and Thomas Giorgio for their contribution to the development of the contact area glass setup. Philippe Vergne, Kees Venner and Bengt Wennehorst for their advice in I-EHL theory. Wojciech Litwin for providing data on the tail shaft dynamic behavior.

Conflicts of Interest: The authors declare no conflict of interest.

Nomenclature

ω	Shaft angular velocity	[rad/s]
ε	Radial misalignment (offset)	[m]
θ	Angular misalignment (slant)	[°]
x, y	Coordinate system in the circumferential and axial directions	[m]
S_q	Root mean square roughness	[m]
$\lambda_{x/y}$	Root mean square wavelength in the circumferential and axial directions	[m]
$\Delta_{x/y}$	Root mean square slope in the circumferential and axial directions	[−]
$R_{x/y}$	Effective radius of curvature in the circumferential and axial directions	[m]
A	Amplitude of the equivalent sinusoidal roughness profile	[m]
$N_{x/y}$	Number of asperities in the circumferential and axial directions	[−]
u_x	Mean surface velocity in the circumferential direction	[m/s]
w_z	Average normal load per asperity	[N]
E'	Equivalent elastic modulus	[Pa]
W_x	Dimensionless load parameter	[−]
U_x	Dimensionless velocity parameter	[−]
h_{cen}	Central film thickness	[m]
h_{min}	Minimum film thickness	[m]
F	Normal load (radial seal load)	[N]
E	Young modulus	[Pa]
ν	Poisson ratio	[−]
ρ	Density	$\left[\mathrm{kg/m^3}\right]$
C_p	Specific heat capacity	[J/(kg·K)]
k	Thermal conductivity	[W/(m·K)]
α_T	Thermal expansion coefficient	[1/K]
η	Dynamic viscosity of the lubricant	[Pa·s]
h	Fluid film thickness	[m]
p	Hydrodynamic pressure	[Pa]
p_c	Cavitation pressure	[Pa]
ρ_c	Density of the lubricant in the cavitation region	$\left[\mathrm{kg/m^3}\right]$
β	Bulk modulus of the lubricant	[Pa]
ϕ	Dimensionless cavitation variable	[−]
g	Cavitation index	[−]
L_c	Width of the contact	[m]
T	Temperature	[°C]
t	Time	[s]

References

1. Jagger, E.T. Rotary Shaft Seals: The Sealing Mechanism of Synthetic Rubber Seals Running at Atmospheric Pressure. *Proc. Inst. Mech. Eng. Part J J. Eng. Tribol.* **1957**, *171*, 597–616. [CrossRef]
2. Johnston, D.E.; Vogt, R. Rotary shaft seal friction, the influence of design, material, oil and shaft surface. *SAE Tech. Pap.* **1995**, *2*, 1453–1466.
3. Stakenborg, M.J.L. On the sealing mechanism of radial lip seals. *Tribol. Int.* **1988**, *21*, 335–340. [CrossRef]
4. Wennehorst, B. *On Lubrication and Friction in Soft Rough Conformal Sliding Contacts*; Leibniz Universität Hannover: Hannover, Germany, 2016.
5. Salant, R.F. Theory of lubrication of elastomeric rotary shaft seals. *Proc. Inst. Mech. Eng. Part J J. Eng. Tribol.* **1999**, *213*, 189–201. [CrossRef]

6. Muller, H.K.; Nau, B.S. Rotary Lip Seals. In *Fluid Sealing Technology: Principles and Applications*; Marcel Dekker Inc.: New York, NY, USA, 1998.
7. Kawahara, Y.; Abe, M.; Hirabayashi, H. An Analysis of Sealing Characteristics of Oil Seals. *Asle Trans.* **1980**, *23*, 93–102. [CrossRef]
8. Horve, L.A. *Shaft Seals for Dynamic Applications*; Marcel Dekker Inc.: New York, NY, USA, 1996.
9. Mokhtar, M.O.A.; Mohamed, M.A.A.; El-Giddawy, M.E.; Yassen, S.A.Y. On the effect of misalignment on the performance of U-type lip seal. *Wear* **1998**, *223*, 139–142. [CrossRef]
10. Arai, Y. Sealing theory in oil seals. In Proceedings of the JSLE-ASLE International Lubrication Conference, Tokyo, Japan, 9–11 June 1975; pp. 830–839.
11. Stakenborg, M.J.L. Visco-Elastohydrodynamic (VEHD) Lubrication in Radial Lip Seals: Part 1-Steady-State Dynamic Viscoelatic Seal Behavior. *Trans. ASME* **1990**, *112*, 578. [CrossRef]
12. Van der Vorst, B.; Organisciak, M. Fast Analytical Model for Followability Prediction of Rotary Shaft Seals. In Proceedings of the 19th International Sealing Conference, Stuttgart, Germany, 12–13 October 2016.
13. Poll, G.; Gabelli, A. Formation of Lubricant Film in Rotary Sealing Contacts: Part I—Lubricant Film Modeling. *J. Tribol.* **1992**, *114*, 280–287. [CrossRef]
14. Borras, F.X.; Bazrafshan, M.; De Rooij, M.B.; Schipper, D.J. *Stern Tube Seals under Static Condition: A Multi-Scale Contact Modelling Approach*; University of Twente: Enschede, The Netherlands, 2019.
15. Tasora, A.; Prati, E.; Marin, T. A method for the characterization of static elastomeric lip seal deformation. *Tribol. Int.* **2013**, *60*, 119–126. [CrossRef]
16. Pinedo, B.; Aguirrebeitia, J.; Conte, M.; Igartua, A. Tri-dimensional eccentricity model of a rod lip seal. *Tribol. Int.* **2014**, *78*, 68–74. [CrossRef]
17. Van Bavel, P.G.M. The Leakage-Free Operation of Radial Lip Seals. Ph.D. Thesis, Eindhoven University, Eindhoven, The Netherlands, 1997.
18. Litwin, W. Experimental Investigation on Marine Main Shaft. In Proceedings of the STLE/ASME 2010 International Joint Tribology Conference, San Francisco, CA, USA, 17–20 October 2010; pp. 1–3.
19. Sinzara, W.; Sherrington, I.; Smith, E.H.; Brooks, H.; Onsy, A. Effects of Eccentric Loading on Lip Seal Performance. In Proceedings of the 6th European Conference on Lubrication Management and Technology (Lubmat 2018), San Sebastián, Spain, 5–6 June 2018.
20. Organisciak, M.; Baart, P.; Paykin, A. Theoretical and experimental study of the frictional losses of radial shaft seals for industrial gearbox. In Proceedings of the AGMA Fall Technical Meeting, Arlington, VA, USA, 12–14 October 2014; pp. 154–165.
21. Hamrock, B.J.; Schmid, S.R.; Jacobson, B.O. *Fundamentals of Fluid Film Lubrication*; CRC Press: Boca Raton, FL, USA, 2004; pp. 504–538.
22. Fowell, M.T.; Myant, C.; Spikes, H.A.; Kadiric, A. A study of lubricant film thickness in compliant contacts of elastomeric seal materials using a laser induced fluorescence technique. *Tribol. Int.* **2014**, *80*, 76–89. [CrossRef]
23. Nijenbanning, G.; Venner, C.H.; Moes, H. Film thickness in elastohydrodynamically contacts. *Wear* **1994**, *176*, 217–229. [CrossRef]
24. Gabelli, A. Micro-elastohydrodynamic lubricant film formation in rotary lip seal contacts. *Tribol. Ser.* **1989**, *14*, 57–68.
25. Chittenden, R.J.; Dowson, D.; Taylor, C.M. Paper VIII(ii) The lubrication of elliptical conjunctions in the isoviscouselastic regime with entrainment directed along either principal axis. *Tribol. Ser.* **1987**, *11*, 247–260.
26. Koukoulopoulos, E.; Papadopoulos, C.I. Piston ring performance in two-stroke marine diesel engines: Effect of hydrophobicity and artificial surface texturing on power efficiency. *Proc. Inst. Mech. Eng. Part J J. Eng. Tribol.* **2018**, *232*, 940–963. [CrossRef]
27. Kalsi, M.S.; Fazekas, G.A. *Feasibility Study of a Slanted O-Ring as a High Pressure Rotary Seal*; ASME Paper 72-WA/DE-14; ASME: New York, NY, USA, 1972.

28. Roemen, R. Calculations on the Oil Film Between a Propeller Shaft and the Aft Sterntube Bearing. In *Polar and Arctic Sciences and Technology*; Offshore Technology: Beijing, China, 2011; Volume 1, pp. 815–821.
29. Silvestri, M.; Prati, E.; Tasora, A. Numerical Analysis of Sealing Conditions in Elastomeric Rings. In Proceedings of the IV AIMETA International Tribology Conference Proceedings, Rome, Italy, 14–17 September 2004; pp. 509–606.